

Anomalous saturation effects due to optical spin depolarization in nitrogen-vacancy centers in diamond nanocrystals

Robert Chapman and Taras Plakhotnik*

School of Mathematics and Physics, The University of Queensland, QLD 4072, Australia

(Received 1 April 2011; revised manuscript received 8 March 2012; published 10 July 2012)

The photoluminescence of the negatively charged nitrogen-vacancy (NV^-) center displays anomalous saturation behavior at high excitation pulse energies. Where the luminescence is expected to approach a maximum value asymptotically, we have found that it instead drops by as much as a factor of two. In this report, we present evidence that these effects are caused by optical spin depolarization of the NV^- center. We show that the presence of an external magnetic field results in a marked decrease in the anomalous character of the NV^- centers' luminescence and demonstrate that low-energy pulses applied after a strong depolarizing pulse can repolarize the spin of the center. We also offer a model and derive important parameters describing dynamics in the NV center and its interaction with light, which quantitatively explain all the observations.

DOI: [10.1103/PhysRevB.86.045204](https://doi.org/10.1103/PhysRevB.86.045204)

PACS number(s): 78.67.Bf, 76.30.Mi, 78.47.-p, 78.55.-m

I. INTRODUCTION

Nitrogen-vacancy (NV) centers¹ are defects of the diamond crystal lattice made of a vacancy and an adjacent substitutional nitrogen atom. NV centers occur naturally in small concentrations but these concentrations can be increased dramatically by irradiating crystals with high-energy electrons, protons, or alpha-particles, followed by annealing at around 800 °C.¹ NV centers have recently attracted interest in many areas of research due to their magneto-sensitivity,² photostability,³ and chemical inertia.⁴ The zero-phonon line at 1.945 eV in the photoluminescence spectrum of the negatively charged center is attributed to a strong dipole transition between its spin-triplet ground and excited states. The centers have a large absorption cross section of $1.0 \pm 0.3 \times 10^{-16}$ cm² at a practically convenient 532-nm wavelength.⁵ These unique properties make the NV center a promising candidate for various applications.⁶ The ground state has a total spin of 1 and nano-magnetometry, based on the sensitivity of the spin to the external magnetic fields, was first proposed as a theoretical concept⁷ and later demonstrated experimentally.^{8,9} Quantum information processing¹⁰⁻¹³ and biomedical applications¹⁴⁻¹⁶ are also hot topics, and the provided references give several examples in the area. In recent papers, it has also been demonstrated that nano-diamonds can be used as nanoscale temperature-sensors^{17,18} and electric field sensors.¹⁹ The photostability of NV centers depends on the crystal size, and centers in ultrasmall (about 5 nm across) diamonds are subject to luminescence intermittency.²⁰ A lot of interest exists in fabrication of NV centers at high concentration²¹⁻²⁴ and in ultrasmall 5-nm diamond crystals.²⁵⁻²⁷

In this paper, we investigate a new phenomenon recently reported²⁸ that manifests itself as a drop in luminescence intensity of centers excited by a pulsed laser, when the excitation energy density of the excitation pulse increases. It is expected that the luminescence of the NV centers should rise linearly with laser excitation at very low energies, followed by a decrease in the growth rate as the NV in diamond asymptotically approaches its maximum luminescence, which is achieved when a center is excited with probability 1 by each pulse. When the pulse length is much shorter and the delay between the pulses are much longer than the relaxation times

in the NV center, saturation of the signal R can be described by a simple two-parameter equation^{5,28}

$$R = R_{\infty}[1 - \exp(-E/E_{\text{sat}})] \quad (1)$$

where R_{∞} is the asymptotic value of the photon detection rate, dependent on the quantum yield of the luminescence and the photon detection efficiency of the experimental apparatus. E is the energy of a single laser-pulse, and E_{sat} is a parameter called the saturation energy.^{5,28} It was most surprising to find significant deviations from Eq. (1). We associate this observation with a new manifestation of spin polarization (preferred population of a certain spin sublevel) in NV centers. The dynamics of the spin in NV centers is pivotal for many applications, and this work adds to the field a new feature. The regime of strong excitation of NV centers is used for a number of applications, such as stimulated emission depletion microscopy.¹⁵ Better understanding of strong-excitation effects in NV centers is therefore important for the advancement of these fields. Finally, the analysis of the results described in this paper allows obtaining information about relaxation rates and the photoionization cross section of the center.

II. SPIN OF NV CENTERS AND LUMINESCENCE

The total spin of an NV^- center in its ground electronic state is 1; therefore, it can have three possible projections, $m = 0$ and $m = \pm 1$ on the axis connecting the nitrogen atom and the vacancy (see Fig. 1). The zero-field splitting between the $m = 0$ and $m = \pm 1$ levels is approximately 2.83 GHz in the electronic ground state. Under normal conditions at room temperature, all three spin sublevels are equally populated. Although absorption of a photon and relaxation to the ground state through photoluminescence does not change the value of m because of the selection rules of the radiative electric-dipole transition, a process initiated by light absorption transfers the spin population from $m = \pm 1$ states to the $m = 0$ state. This process is called optically induced spin polarization. The accepted model of spin polarization assumes that the states $m = \pm 1$ can relax nonradiatively to the ground state via an intermediate singlet electronic state (this state is situated

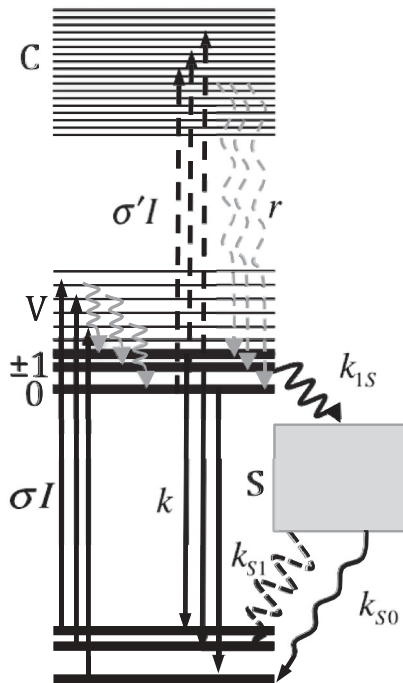


FIG. 1. Simplified energy diagram of an NV center. The straight lines represent radiative transitions (absorption and emission of a photon). Wavy lines symbolize nonradiative transitions. Solid lines sketch the conventional path for transferring a population from $m = \pm 1$ states to $m = 0$ states, and the dashed lines represent transitions proposed in this paper to explain our experimental observations (they transfer a part of the population from $m = 0$ back to $m = \pm 1$). All singlet states are shown as a gray box and labeled S. Label C stands for conduction band and V for the vibronic states. The absorption rates from the ground and the excited electronic states are σI and $\sigma' I$, respectively, with I being the laser intensity and σ , σ' the corresponding absorption cross sections.

between the two triplet states) and that the singlet state then relaxes predominantly to the $m = 0$ level of the ground state.^{29,30} The described nonradiative path is very inefficient for the $m = 0$ state, causing it to relax primarily via the photoluminescence path. A center polarized to the $m = 0$ state will therefore have a greater photoluminescence intensity than a depolarized center.² Although 100% spin polarization is highly desirable for applications, only about 85% population of the $m = 0$ state has been reported in the literature. It is believed but not confirmed experimentally that the limit of 85% is set by the nonzero probability of the spin-changing optical transitions.³⁰ A hot topic in the literature is the detailed mechanism of such spin polarization. In particular, the number of singlet states involved and their symmetry has been a subject of scrutiny.^{30–35} The general consensus is that the electronic ground term is of 3A_2 symmetry (C_{3v} point group) and the excited spin-triplet is an orbital-doublet (E_x, E_y). The doublet is split because of a linear strain in the crystal.³⁶ This splitting is less than 100 GHz but can be observed at low temperatures. However, electronically excited states are generally not well understood. The unresolved questions are the number of singlet states between the two lowest triplet states, their symmetry, and the selection rules for the spin-polarizing intersystem crossing (ISC). The number of singlet states ranges between one and

three in different models. For example, three singlet states ${}^1E'$, 1A , and 1E (in order from the highest to the lowest) were recently predicted using *ab initio* many-body perturbation theory.³⁴

III. EXPERIMENTAL

The experimental apparatus⁵ is based on a wide-field epifluorescence microscope. This allows observation of several crystals simultaneously. We focus 532-nm light from a pulsed-output fiber laser (Fianium) with a pulse duration of 80 ps through a prefocusing lens and a microscope objective (Nikon, NA 0.9 \times 100) to form a spot approximately 30 μm in diameter on a quartz slide spin-coated with diamond nanocrystals. These crystals have an average size of 30 nm and were purchased from the Academia Sinica production facility. NV centers were produced by irradiation of diamond nanocrystals with He^+ ions followed by annealing as described in the literature.²³ Luminescence from NV^- centers is collected by the microscope objective and sent to a detector. Depending on the experiment, for detection we used either a thermoelectrically cooled Electron Multiplying CCD (Andor iXon) or a time-gated Image-Intensified CCD (Stanford Computer Optics 4Picos), which has a sub-nanosecond time resolution. Both detectors were used in conjunction with either a spectrometer (Acton SP2300) or a set of filters that transmit the emission of negatively charged NV^- in the 675–700-nm band and block both background light and light from the NV^0 species, whose luminescence is centered around 630 nm. A magnetic field used in one of the experiments was created by a small permanent magnet. The direction of the field was parallel to the optical axis of the microscope objective and perpendicular to the substrate with the diamond crystals.

Dependence of the photoluminescence rate on the energy of the laser pulses is shown in Fig. 2. The experimental data accurately follows Eq. (1) at relatively low pulse energies, but when the pulse energy is approximately five times the saturation energy, the experimental points deviate significantly from the theoretical prediction. For this crystal, luminescence intensity levels out at approximately 75% of its maximum value as the pulse energy increases. The emission rate decreases 1.7 times compared with the predictions of Eq. (1). The saturation curve was measured by taking half of the measurements going from low-energy to high-energy pulses, and the other half using decreasing pulse energy. The luminescence spectra shown in Fig. 3 were measured at the pulse energy of 0.08 μJ (this energy corresponds to the peak of the curve shown in Fig. 2) and at 1 μJ .

The curve remained consistent regardless of whether it was measured using increasing or decreasing pulse energy, suggesting some mechanism by which the luminescence recovers after being affected by the high-energy laser pulses. We used amplitude-modulated excitation pulses to investigate the dynamics of this recovery. The pulse sequence had a period of 10 μs (see Fig. 4, insert). The sequence started with a relatively strong “dimming” pulse, the energy of which varied in a wide range. After this pulse, there were N “luminescence-recovering” pulses. The energies of these pulses were always E_m . The value E_m was chosen to be close to the energy at the peak of the saturation curve in Fig. 2. Typically this energy

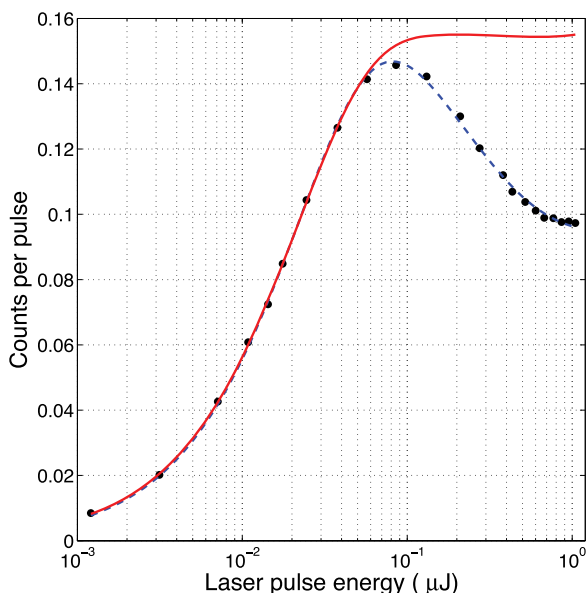


FIG. 2. (Color online) Photoluminescence of NV^- centers at different energies of the exciting laser pulse (pulse repetition rate is 1 MHz). The smooth solid curve is obtained by fitting Eq. (1) to the first eight low-energy points. The saturation energy is $0.02 \mu J$. The dashed line is a fit to a model as explained later in the paper.

was three to five times the saturation energy. The dependence of the average NV luminescence intensity on the energy of the first pulse and the number of the recovering pulses is shown in Fig. 4. The detected signal is divided by the number of pulses per period of the pulse sequence. For example, in the case of one strong pulse followed by three weaker pulses, the signal

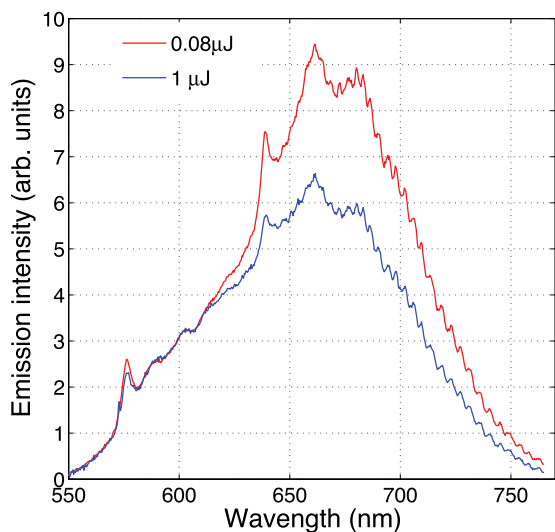


FIG. 3. (Color online) Spectra of an ensemble of NV centers in a nanocrystal at two different pulse energies. The intensity units are the same for both spectra. The spectrum with higher intensity is measured at $0.08 \mu J$, and the lower spectrum is measured at $1 \mu J$ of the excitation-pulse energy. These energies are significantly above the saturation energy of $0.02 \mu J$. In this saturation regime, there is no significant change in NV^0 emission, but the decrease in NV^- emission is clearly visible.

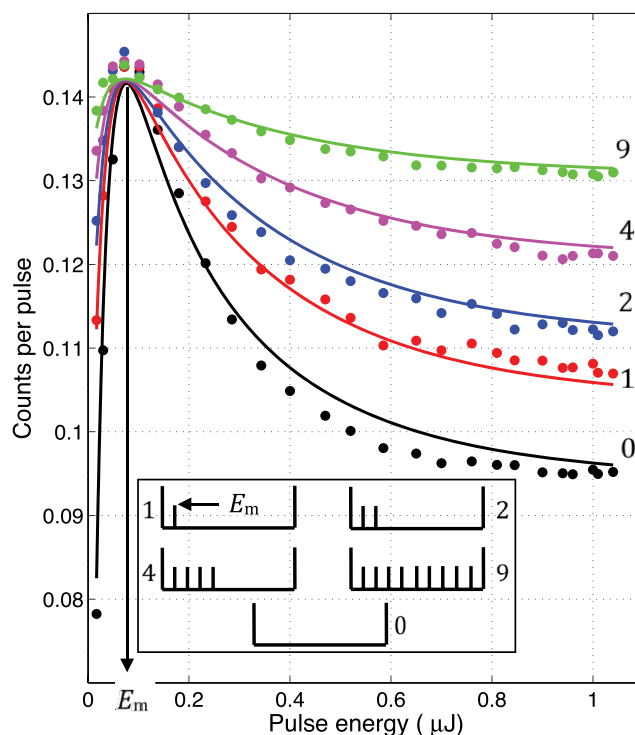


FIG. 4. (Color online) Spin polarization can be recovered using low-energy pulses after the initial high-energy depolarizing pulse. The pulse energy in the figure is the energy of the first pulse in the sequence (periodically repeated). The energy of the following pulses was always E_m . The dots are experimental points, and the solid line is the best fit to the model (see Table I for fitted parameters). The inset shows schematically the pulse sequences used to obtain each of the curves.

has been divided by a factor of four. Such scaling takes into account the trivial increase in photoluminescence rate because more excitation pulses are shot within the $10\text{-}\mu s$ time intervals. As can be seen from Fig. 4, the drop of luminescence gradually decreases when the number of recovering pulses increases.

The magnitude of the intensity drop also reduces significantly when the crystal is placed in an external magnetic field. This is shown in Fig. 5. The magneto-optical effect clearly points to the important role played in this effect by the spin of the NV centers.^{37–39} In particular, the external magnetic field induces mixing of the spin state and thus decreases the level of spin polarization.

The luminescence decay of the NV centers after the laser-pulse at various excitation energies is shown in Fig. 6. Luminescence decay was measured at excitation energy corresponding to the linear portion of the saturation curve, at its peak, and at the maximum pulse energy. The luminescence was integrated on the Image-Intensified CCD for a time interval of 40 ns with varying delays after the laser pulse. The magnetic field’s effect on the decay was also examined. As can be seen from Fig. 6, all luminescence decay curves can be approximated very well with two exponential functions. Note that the high-rate component becomes more prominent at high pulse energy, and at any pulse energy in the presence of a magnetic field.

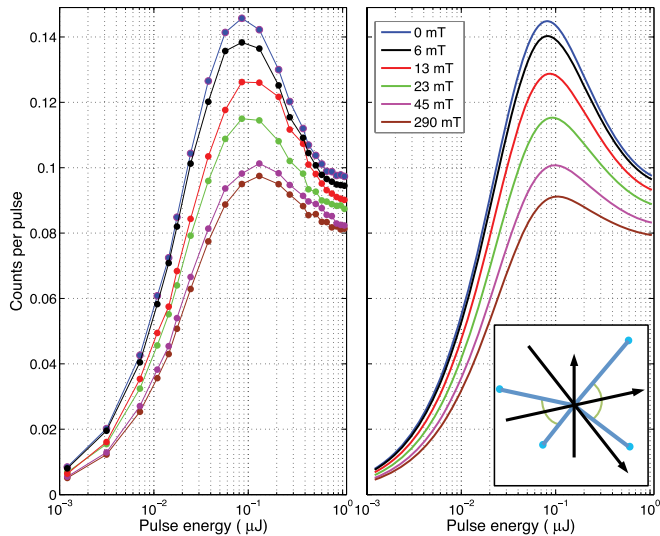


FIG. 5. (Color online) Left panel: saturation curves gathered with external fields between 0 and 290 mT (the field values are shown on the right panel). Right panel: theoretical fits of the data shown on the left. Fits were derived from the model described above. From the data, it is clear that externally depolarized centers show a marked decrease in anomalous saturation behavior. The insert shows the four possible orientations of the NV centers. For the best fit, the magnetic field was oriented approximately along one of these directions. The angles indicated are 109.4° .

IV. DISCUSSION AND MODEL DESCRIPTION

The drop in luminescence intensity could be related to photo-induced conversion of the negatively charged centers to their neutral form. Photoionization of NV^- centers has been experimentally investigated previously.^{40,41} Interestingly, phototransformation of NV^0 to NV^- has also been reported⁴² and explained by ionization of an impurity whose electron is then captured by NV^0 . The spectra in Fig. 3 demonstrate that while the emission of the negatively charged NV center (distinguishable by its 638-nm zero-phonon line and a phonon band with a maximum at about 680 nm) decreases by a factor of 1.5, the spectrum of the neutral center (with a zero-phonon line at ~ 575 nm) remains unchanged. Therefore, the mechanism of the observed decrease in the NV^- emission does not agree with the kinetics described in previous publications^{40,42} reporting the photo-induced interconversion of NV^- and NV^0 where the diminishing luminescence of one type of center has been accompanied by a corresponding increase in the luminescence of the other center.

It has also been documented that the luminescence intensity of NV centers drops as the temperature increases significantly above room temperature.¹⁷ But as the temperature increases, the zero-phonon lines associated with both negatively charged and neutral NV centers broaden and become indistinguishable from the background of the phonon band above 500 K.¹⁷ However, little broadening (less than 30%) has been observed in these experiments, as shown by the spectra in Fig. 3. We conclude that the average temperature of the crystal is less than 400 K, which rules out a significant temperature-related effect.

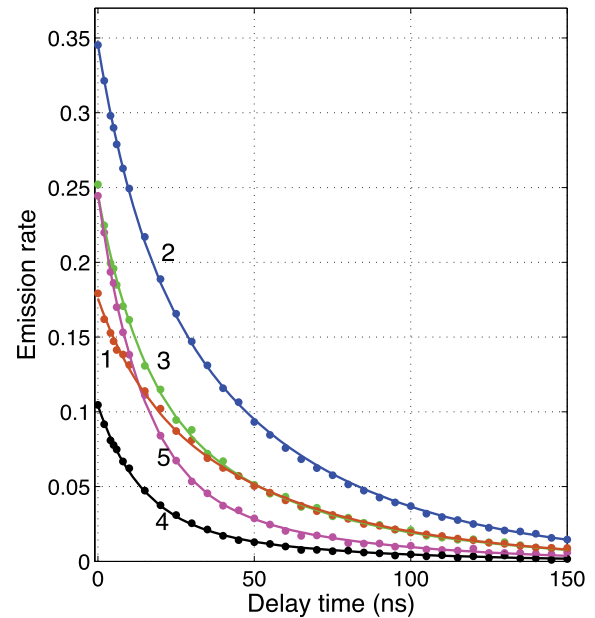


FIG. 6. (Color online) Luminescence decay curves gathered at three different pulse energies: $0.013 \mu\text{J}$ (curve 1), $0.085 \mu\text{J}$ (curve 2), and $1.1 \mu\text{J}$ (curve 3). In the presence of an external magnetic field of 290 mT, curves were measured at pulse energies of $0.013 \mu\text{J}$ (curve 4) and $1.1 \mu\text{J}$ (curve 5). We found that all decay curves can be fitted with a two-exponential decay. The decay rates and the amplitudes of the fast/slow components for curve 1 are $57(7)/18(1)$ MHz and $0.059(8)/0.115(9)$, curve 2, $61.4(3)/17.9(3)$ MHz and $0.126(6)/0.216(6)$; curve 3, $85(5) / 18.9(6)$ MHz and $0.130(5)/0.117(5)$; curve 4, $70(3)/20(2)$ MHz and $0.074(4)/0.029(4)$; curve 5, $70(2)/17(1)$ MHz and $0.195(5)/0.050(5)$, where the numbers in brackets show the standard deviation of the last digit (e.g., the amplitude of the fast component of curve 5 is 0.195 and the standard deviation is 0.005). The increased significance of the faster decaying component at higher energies of the pulse is clearly visible when comparing curves 1 and 3. The presence of the magnetic field also increases the relative contribution of the faster decaying exponent, as can be seen from comparison of curves 3 and 5.

As has already been mentioned, the key to the explanation is provided by the saturation curve measured when the magnetic field was switched on. The curve is then close to the prediction of Eq. (1), and the luminescence intensity at the highest pulse energy is close to the intensity observed without the field. The magnetic field mixes the states with different values of the spin projection on the axis of the NV center^{37–39} and reduces the degree of the spin polarization. Therefore, we can assume that the high-energy laser pulses depolarize the spin state. Obviously this has little effect if the spin is already depolarized by a strong external magnetic field as seen in Fig. 5. Interestingly, the change in the spin polarization does not affect the saturation energy value. This insensitivity of the saturation curve to the population of the metastable states is expected for the short-pulse excitation.²⁸

First, we briefly discuss a well-known spin depolarization mechanism, spin-lattice relaxation. The spin-lattice relaxation rate at room temperature is about 1 kHz, but above room temperatures, it quickly increases, proportional to the fifth power of the temperature.⁴³ It is therefore possible that spin

TABLE I. Parameters derived by fitting the model to the experimental data.

σ	$0.95 \times 10^{-16} \text{cm}^2$
σ'	$6.5 \times 10^{-18} \text{cm}^2$
k_{1S}	43 MHz
k_{S1}	0.9 MHz
k_{S0}	2.4 MHz
k	20 MHz
r	$\gg 20$ MHz

is depolarized due to an increase in the crystal temperature. Although the average temperature does not change significantly under high-pulse energy excitation, as indicated by the zero-phonon line, a high temperature may still be present in the crystal for only a small fraction of the luminescence lifetime, but achieving the thermal equilibrium of the spin states within a few nanoseconds requires unrealistically high temperatures (10 times higher than room temperature) and therefore can be excluded.

Our model is based on the idea of an electronically excited C state, reachable from the excited state using 532-nm excitation. This state has triplet multiplicity as it is radiatively coupled to the excited triplet state, although the purity of its triplet origin may be somewhat affected by the spin-orbit coupling. According to the Kasha and Kasha-Vavilov rules,⁴⁴ the most probable relaxation path from state C is fast nonradiative relaxation to the lowest excited state of the same multiplicity, the first excited triplet state (see also discussion of the luminescence decay rates below). The only assumption that we make about the nature of state C is that the strength of the spin-orbit coupling is sufficient to substantially diminish spin polarization when the electron in state C relaxes to the lowest excited triplet state. Because the first excited state of the NV^- center is close to the conduction band, the ionized state of NV^- is a likely candidate for the C state. In the two-step photoionization of NV^- , the electronic configuration of the center changes as follows $a_1^2 a_1^2 e^2 \rightarrow a_1^2 a_1^1 e^3 \rightarrow a_1^2 a_1^1 e^2$. A fast rate of the subsequent recombination ensures that NV^0 created in this process does not contribute to the luminescence spectrum. Note that the fast nonradiative relaxation from the C state to the lowest excited triplet state is enabled through effective conversion of the electronic energy difference into vibrational energy of the lower electronic state.⁴⁵ Strong vibronic coupling can also substantially increase spin-orbit interactions.⁴⁶ For simplicity of modeling, we assumed that the C state decays to each spin component of the first excited triplet state at the same rate. Note that the resulting behavior of the emission rate will not change if the “free” electron in state C is captured by another (not parental) neutral NV center present in the same crystal.

To make the comparison between the experiment and our explanation quantitative, we have solved rate equations similar to those used by Rogers *et al.*³⁸ The involved rates are shown in Fig. 1, and the details are explained in the Appendix. By solving the rate equation, we were able to find the parameters of the model (see Table I). The factors that most strongly affect the theoretical curves in Figs. 4 and 5 are actually the ratios σ/σ' , k_{1S}/k , and k_{S1}/k_{S0} . The value of the absorption cross

section σ was published recently,⁵ and it has been used to estimate the absorption cross section from the excited triplet to the C state. The radiative rate k depends on the orientation of the transition dipole relative to the glass-air interface. When the dipole moment is parallel to the interface, the emission decays 1.7 times slower than when it is perpendicular to the interface plane.⁴⁷ We have used 20 MHz as an estimate for the radiative rate. This choice has been motivated by the results of the luminescence decay measurements (see below). The ISC rate from the triplet ($m = \pm 1$) to the singlet (see Fig. 1) turned out to be significantly faster in our sample than measured previously in bulk diamond.³⁰

The model successfully explains the recovery of spin polarization. First, we have used chi-squared criteria to find the best agreement between the data in Fig. 4 and the model. The fitting minimizes the value of $\chi^2 = \sum (R_e - R_m)^2$, where R_e and R_m are, respectively, the luminescence rates detected experimentally and calculated using the suggested model. The best agreement is achieved when $k_{S1}/k_{S0} \approx 0.6$. If the data in Figs. 4 and 5 are fitted together (the fits are shown in the figures), then the optimal ratio of $k_{S1}/k_{S0} \approx 0.4$. The value of the chi-square increases by a factor of two in each of these cases, if we keep the value of k_{S1} at zero (the value suggested in the literature) when running the optimization algorithm. Therefore, we conclude that the singlet state relaxes with comparable probabilities to the $m = 0, \pm 1$ levels in the electronic ground state. The rate of 3.3 MHz for the relaxation from the singlet reported by Manson *et al.*³⁰ is actually the total rate of the singlet depopulation. Using this number and the ratio of 0.4, we determine that $k_{S1} \approx 0.9$ MHz and $k_{S0} \approx 2.4$ MHz.

The model explains the effect of the magnetic field reasonably well if the orientation of the crystal relative to the field is used as a fitting parameter. The strength of the emission observed from this crystal corresponds to approximately 50 NV centers, and we assumed that there are an equal number of NV centers oriented along each of the four possible directions within the crystal. This assumption has made the model moderately sensitive to crystal orientation. Other authors^{38,39} report significant deviations between the theoretical dependence of the luminescence intensity on the magnetic field and the experiment. The reason for the $\sim 10\%$ discrepancy as reported by Rogers *et al.*³⁸ is not clear. In our case, the largest discrepancy of about 6% is observed for the strongest magnetic field. This indicates that the model misses some minor effects but correctly describes major trends. The fit could be improved by adding the populations of the four orientations of the NV centers and a distribution of lifetimes to the fitting parameters.

The model also explains the behavior of the luminescence decay curves. We find that the data are consistent with a two-exponential decay

$$R = A_1 \exp(-k_1 t) + A_2 \exp(-k_2 t) \quad (2)$$

where k_1 and k_2 are the decay rates of the two components. A_1 and A_2 are the corresponding amplitudes proportional to $p_1 [1 - \exp(-k_1 t_i)] k_1^{-1}$ and $p_2 [1 - \exp(-k_2 t_i)] k_2^{-1}$, where p_1 and p_2 are the populations of the states. Additional factors take into account the effect of integration over $t_i = 40$ ns on the chip of the Image-Intensified CCD. The decay rates (see

caption of Fig. 6) are close to the transition rates determined by fitting the model: 63 MHz for the $m = \pm 1$ states and 20 MHz for the radiative transition from $m = 0$. Our model is further supported by the fact that the values $p_1 + p_2$ are the same within the accuracy of measurements for curves 2, 3, and 5, the curves obtained when absorption from the ground state is completely saturated. This confirms that the decrease in luminescence intensity when power increases from 0.085 to 1.1 μJ or when the magnetic field is switched on is not related to the decrease in the total population of the excited states whose radiative decay contributes to the luminescence signal (as has been already concluded from the spectra in Fig. 3). In particular, nonradiative relaxation to the ground electronic state directly from the C state would decrease the value of $p_1 + p_2$. In agreement with the model is also the increasing of the relative amplitude of the fast decaying term in Eq. (2) as the degree of the spin depolarization increases.

The simulated data depend very little on the relaxation rate from the C state. Therefore, we can only set a low limit on the value of r (see Fig. 1), exploiting the fact that the slowest decay rate in Fig. 6 is 18 MHz and that the time-resolved data integrated for 40 ns agree well with the data in Fig. 5, which were obtained after integration for several seconds. For example, the value of $A_1/[1 - \exp(-k_1 t_i)] + A_2/[1 - \exp(-k_2 t_i)]$ for curve 2 is about 1.4 times larger than for curve 3. This is close to 1.5, the ratio measured with the same pulse energies but without time gating, and shows that no long-lived components (except for the two identified by the fitting the decay curves) contribute significantly to the averaged luminescence signal.

It is interesting to discuss our results in the context of two other experiments performed in bulk diamond and related to the photoionization of NV^- . In an earlier experiment,⁴¹ the photoionization process had been accompanied by the corresponding increase in the emission of NV^0 . The efficiency of this ionization was estimated to be 10^{-3} . If a center cycles 1000 times before changing its charge state, the spin polarization would practically always be at maximum since it takes only a few cycles to repolarize the spin, even if it were depolarized after the ionization. Also, the photoionization was spontaneously reversible with a representative time constant of about 10 μs . If the NV^0 created by the photoionization had such a long lifetime, then ionization of NV^- would increase emission in the spectral region of NV^0 . Such an increase is not observed in our experiment. Therefore, we conclude that the ionization process proposed by Manson and Harrison⁴¹ plays a minor role (if any) in our crystals. Recently, two-photon excitation of NV^- followed by an Auger process, absorption of two other photons, and capturing an electron from the valence band of the crystal have been proposed⁴⁸ to explain experiments in ultrapure bulk diamond at low temperatures. Reflecting on this line of thought, we note that the electron configuration of the neutral center created by the transformation $a_1^2 a_1^1 e^3 \rightarrow a_1^2 a_1^1 e^2$ could be simply converted into $a_1^1 a_1^2 e^2$ and then $a_1^2 a_1^1 e^2$, the ground state of NV^- , first by absorbing just one photon and promoting an electron from the lowest $a_1(1)$ state, which is about 1.2 eV below the maximum energy of the valence band and 2.6 eV below the energy of $a_1(2)$ ³⁵, and then by capturing an electron from the valence band into the depopulated $a_1(1)$ state. The

kinetics of this process will be similar to that discussed in this paper if three conditions are fulfilled. First, the key assumption is that during the photoionization stage or in the transformation of NV^0 back to NV^- the spin polarization of the NV center is lost. Second, the step $a_1^2 a_1^1 e^3 \rightarrow a_1^2 a_1^1 e^2$ should be the slowest process in the closed loop of the NV transformations to ensure that the most probable state of the center at the end of a strong laser pulse is the excited-triplet $a_1^2 a_1^1 e^3$. Third, the energy of a photon at 532-nm wavelength (2.3 eV) should match the gap between $a_1(2)$ and $a_1(1)$. Summarizing the paragraph, we believe that the model suggested in this paper is essentially distinctive from other proposals in the field while being convincingly supported by the presented experimental data.

V. CONCLUSION

In this work, we have analyzed the anomalous saturation behavior of the negatively charged NV centers and have shown that the drop in luminescence intensity as the energy of the exciting laser pulse increases cannot be related to the decrease in the time-averaged number of NV^- centers in the crystal. We demonstrate that our experimental results agree well with the model in which optically induced spin depolarization (and the related increase of the radiationless ISC) is the mechanism responsible for the reduction of the photon emission rate. This mechanism has been confirmed by using an external magnetic field that reduces spin polarization in the NV^- centers by spin mixing. The suggested optical spin depolarization results from a process that consists of two-photon excitation of the center to state C (placed in the conduction band of the crystal) followed by fast return of the center to the first excited triplet state of NV^- . The exact nature of the C state and the related dynamics warrant further theoretical and experimental investigations. Finally, we have shown that a series of low-power pulses following an initial high-power pulse can cause the luminescence of the NV^- center to recover, a finding that is in line with our model. The model is most consistent with the experimental data if the ISC rate from the excited triplet to the singlet is about two times faster than the radiative transition rate and (unlike what is commonly accepted) the metastable singlet can relax to the $m = \pm 1$ ground states with rates that are about half the relaxation rate of the $m = 0$ level.

ACKNOWLEDGMENTS

The authors acknowledge useful practical hints from N. B. Manson and financial support from ARC (grant DP0771676).

APPENDIX

We consider a 10-state scheme. The triplet states are labeled using Greek characters, with a number of primes indicating the level of electronic excitation. For example, $|\alpha\rangle$, $|\beta\rangle$, and $|\gamma\rangle$ represent the ground electronic state. The single-primed and double-primed subscripts correspond to the first electronically excited triplet state and the double-excited electronic state (C state), respectively. The singlet state is denoted as $|s\rangle$. The rate equations for the population of these states are shown below

explicitly,

$$\frac{d}{dt} \begin{pmatrix} n_\alpha \\ n_\beta \\ n_\gamma \\ n'_\alpha \\ n'_\beta \\ n'_\gamma \\ n_s \\ n_{\alpha''} \\ n_{\beta''} \\ n_{\gamma''} \end{pmatrix} = \begin{pmatrix} -k_{\Sigma\alpha} & 0 & 0 & k_{\alpha'\alpha} & k_{\beta'\alpha} & k_{\gamma'\alpha} & k_{s\alpha} & 0 & 0 & 0 \\ 0 & -k_{\Sigma\beta} & 0 & k_{\alpha'\beta} & k_{\beta'\beta} & k_{\gamma'\beta} & k_{s\beta} & 0 & 0 & 0 \\ 0 & 0 & -k_{\Sigma\gamma} & k_{\alpha'\gamma} & k_{\beta'\gamma} & k_{\gamma'\gamma} & k_{s\gamma} & 0 & 0 & 0 \\ I\sigma_{\alpha\alpha'} & I\sigma_{\beta\alpha'} & I\sigma_{\gamma\alpha'} & -k_{\Sigma\alpha'} & 0 & 0 & 0 & r_{\alpha''\alpha'} & r_{\beta''\alpha'} & r_{\gamma''\alpha'} \\ I\sigma_{\alpha\beta'} & I\sigma_{\beta\beta'} & I\sigma_{\gamma\beta'} & 0 & -k_{\Sigma\beta'} & 0 & 0 & r_{\alpha''\beta'} & r_{\beta''\beta'} & r_{\gamma''\beta'} \\ I\sigma_{\alpha\gamma'} & I\sigma_{\beta\gamma'} & I\sigma_{\gamma\gamma'} & 0 & 0 & -k_{\Sigma\gamma'} & 0 & r_{\alpha''\gamma'} & r_{\beta''\gamma'} & r_{\gamma''\gamma'} \\ 0 & 0 & 0 & k_{\alpha's} & k_{\beta's} & k_{\gamma's} & -k_{\Sigma s} & 0 & 0 & 0 \\ 0 & 0 & 0 & \sigma'I & 0 & 0 & 0 & -k_{\Sigma\alpha''} & 0 & 0 \\ 0 & 0 & 0 & 0 & \sigma'I & 0 & 0 & 0 & -k_{\Sigma\beta''} & 0 \\ 0 & 0 & 0 & 0 & 0 & \sigma'I & 0 & 0 & 0 & -k_{\Sigma\gamma''} \end{pmatrix} \begin{pmatrix} n_\alpha \\ n_\beta \\ n_\gamma \\ n_{\alpha'} \\ n_{\beta'} \\ n_{\gamma'} \\ n_s \\ n_{\alpha''} \\ n_{\beta''} \\ n_{\gamma''} \end{pmatrix},$$

where n_α , n_β , and n_γ are the populations of the three spin-related sublevels in the ground electronic state; n'_α , n'_β , and n'_γ are the populations of the three spin-related sublevels in the first excited electronic triplet state; and n''_α , n''_β , and n''_γ are the populations of the three spin-related sublevels in the C state. We neglect the spin-lattice relaxation rates, which are on the order of 1 kHz at room temperatures. Recombination rates from the C state are $r_{\alpha''\alpha'}$, $r_{\beta''\beta'}$ and so on. These transitions will reduce the spin polarizations unless they are all equal to zero, with possible exceptions for $r_{\alpha''\alpha'}$, $r_{\beta''\beta'}$, and $r_{\gamma''\gamma'}$. In our model, all these recombination rates are equal to r and are independent of the external magnetic field. In the absence of the external magnetic field, all the absorption cross sections from the ground electronic state and the corresponding radiative relaxation rates are zeros, with an exception for $\sigma_{\alpha\alpha'} = \sigma_{\beta\beta'} = \sigma_{\gamma\gamma'} = \sigma \neq 0$ and $k_{\alpha'\alpha} = k_{\beta'\beta} = k_{\gamma'\gamma} = k \neq 0$. This selection rule changes when the magnetic field is turned on because of the different spin mixing in the ground and excited triplet states. The absorption from the excited state σ' is the same for all spin-related sublevels of the excited triplet state. The negative rates on the diagonal of the matrix balance the sum of the other rates in the same column. For example, $k_{\Sigma\alpha'} = k_{\alpha'\alpha} + k_{\alpha'\beta} + k_{\alpha'\gamma} + k_{\alpha's} + \sigma'I$.

The Hamiltonian describing the spin-related part of the state wavefunction is $\hat{H} = \hat{H}_0 - \gamma_e \mathbf{B} \cdot \hat{\mathbf{S}}$. The zero-field Hamiltonian reads $\hat{H}_0 = E \hat{S}_z^2$, where the value of E is 2.83 GHz in the ground and 1.43 GHz in the excited states.⁴⁹ The eigenstates of \hat{H} are a superposition of the basis states $|l, m\rangle$ where $m = -1, 0, 1$ and $l = 1$. Therefore, eigenstates of the ground triplet state read

$$|\alpha\rangle = |\Psi_{T1}\rangle a_\alpha |1, -1\rangle + |\Psi_{T0}\rangle b_\alpha |1, 0\rangle + |\Psi_{T1}\rangle c_\alpha |1, 1\rangle,$$

$$|\beta\rangle = a_\beta |\Psi_{T1}\rangle |1, -1\rangle + b_\beta |\Psi_{T0}\rangle |1, 0\rangle + c_\beta |\Psi_{T1}\rangle |1, 1\rangle,$$

and

$$|\gamma\rangle = a_\gamma |\Psi_{T1}\rangle |1, -1\rangle + b_\gamma |\Psi_{T0}\rangle |1, 0\rangle + c_\gamma |\Psi_{T1}\rangle |1, 1\rangle,$$

where $|\Psi_T\rangle$ describes a part of the triplet state wavefunction depending on the space coordinates of electrons and nuclei. Expressions for the electronically excited state are similar (one needs to add primes to all Greek symbols).

The electric-dipole operator \mathbf{r} and spin-orbit interaction $\hat{\mathbf{H}}_{\text{SO}}$ govern the transition rates (radiative and ISC, respec-

tively). The transition rates are modified in the presence of the magnetic field as

$$\sigma_{\alpha\beta'} \propto |\langle \alpha | \mathbf{r} | \beta' \rangle|^2 = \sigma |a_{\alpha'}^* a_{\beta'} + b_{\alpha'}^* b_{\beta'} + c_{\alpha'}^* c_{\beta'}|^2;$$

$$k_{\beta'\alpha} \propto |\langle \alpha | \mathbf{r} | \beta' \rangle|^2 = k |a_{\alpha'}^* a_{\beta'} + b_{\alpha'}^* b_{\beta'} + c_{\alpha'}^* c_{\beta'}|^2;$$

$k_{\alpha's} \propto |\langle \alpha' | \hat{\mathbf{H}}_{\text{SO}} | s \rangle|^2 = k_{1s} (|a_{\alpha'}|^2 + |c_{\alpha'}|^2)$ and similar for the other two rates $k_{\beta's}$ and $k_{\gamma's}$; and

$k_{s\alpha} \propto |\langle s | \hat{\mathbf{H}}_{\text{SO}} | \alpha \rangle|^2 = k_{s1} (|a_\alpha|^2 + |c_\alpha|^2) + k_{s0} |b_\alpha|^2$ and similar for $k_{s\beta}$ and $k_{s\gamma}$.

The ISC to the singlet state can be calculated using two-electron states and the spin-orbit Hamiltonian in the form of $\hat{H}'_{\text{SO}} = \hat{\mathbf{V}}'(\mathbf{r}_1) \cdot \hat{\mathbf{S}}_1 + \hat{\mathbf{V}}'(\mathbf{r}_2) \cdot \hat{\mathbf{S}}_2$ (see, e.g., a recent review by Marian⁴⁶), where the orbital part of the Hamiltonian transforms in the C_{3v} symmetry group of the center like an angular momentum operator. The orbital part of the wavefunction in the excited triplet state is double degenerated in the C_{3v} symmetry. First, we calculate the matrix elements for the x -type function,

$$\begin{aligned} & \langle \Psi_{T1}(\mathbf{r}_1, \mathbf{r}_2) | \langle 1, -1 | \hat{H}'_{\text{SO}} | 0, 0 \rangle | \Psi_S(\mathbf{r}_1, \mathbf{r}_2) \rangle \\ &= \langle \Psi_{T1}(\mathbf{r}_1, \mathbf{r}_2) | \langle \downarrow \downarrow | \hat{\mathbf{V}}'(\mathbf{r}_1) \cdot \hat{\mathbf{S}}_1 \\ & \quad + \hat{\mathbf{V}}'(\mathbf{r}_2) \cdot \hat{\mathbf{S}}_2 | \uparrow \downarrow - \downarrow \uparrow \rangle | \Psi_S(\mathbf{r}_1, \mathbf{r}_2) \rangle \\ &= 2(V'_x, V'_y, V'_z) \cdot \langle \downarrow \downarrow | \hat{\mathbf{S}}_1 | \uparrow \downarrow - \downarrow \uparrow \rangle \\ &= \hbar(V'_x + iV'_y) \end{aligned}$$

and similarly for other spin states,

$$\begin{aligned} & \langle \Psi_{T1}(\mathbf{r}_1, \mathbf{r}_2) | \langle 1, 1 | \hat{H}'_{\text{SO}} | 0, 0 \rangle | \Psi_S(\mathbf{r}_1, \mathbf{r}_2) \rangle \\ &= 2\mathbf{V}' \cdot \langle \uparrow \uparrow | \hat{\mathbf{S}}_1 | \uparrow \downarrow - \downarrow \uparrow \rangle = \hbar(-V'_x + iV'_y). \end{aligned}$$

$\langle \Psi_{T0}(\mathbf{r}_1, \mathbf{r}_2) | \langle 1, 0 | \hat{H}'_{\text{SO}} | 0, 0 \rangle | \Psi_S(\mathbf{r}_1, \mathbf{r}_2) \rangle = 2\mathbf{V}' \cdot \langle \uparrow \downarrow + \downarrow \uparrow | \hat{\mathbf{S}}_1 | \uparrow \downarrow - \downarrow \uparrow \rangle = 2\hbar V'_z = 0$, meaning that the ISC is negligible from $|1, 0\rangle$ to $|0, 0\rangle$. If the magnetic field is not zero and the spin states are mixed, then $|\langle \alpha' | \hat{H}'_{\text{SO}} | s \rangle|^2 = \hbar^2 (|V'_x|^2 (a_{\alpha'} - c_{\alpha'})^2 + |V'_y|^2 (a_{\alpha'} + c_{\alpha'})^2)$ because $a_{\alpha'}$ and $c_{\alpha'}$ can be made real by rotating the coordinate system so that $B_y = 0$.

The ISC rate for the y -type orbital function can be obtained by exchanging x and y in the above expression. And the rate becomes proportional to $\hbar^2 (|V'_x|^2 + |V'_y|^2) (a_{\alpha'}^2 + c_{\alpha'}^2)$ when it is averaged over the two electronically degenerated states.

*taras@physics.uq.edu.au

- ¹G. Davies and M. F. Hamer, *Proc. R. Soc. London A* **348**, 285 (1976).
- ²A. Gruber, A. Drabenstedt, C. Tietz, L. Fleury, J. Wrachtrup, and C. von Borczyskowski, *Science* **276**, 2012 (1997).
- ³C.-C. Fu, H.-Y. Lee, K. Chen, T.-S. Lim, H.-Y. Wu, P.-K. Lin, P.-K. Wei, P.-H. Tsao, H.-C. Chang, and W. Fann, *Proc. Natl. Acad. Sci. USA* **104**, 727 (2007).
- ⁴A. M. Schrand, H. J. Huang, C. Carlson, J. J. Schlager, E. Ōsawa, S. M. Hussain, and L. Dai, *J. Phys. Chem. B* **111**, 2 (2007).
- ⁵R. Chapman and T. Plakhotnik, *Chem. Phys. Lett.* **507**, 190 (2011).
- ⁶K. B. Holt, *Philos. Trans. R. Soc. Lond. A: Math. Phys. Eng Sci* **365**, 2845 (2007).
- ⁷C. L. Degen, *Appl. Phys. Lett.* **92**, 243111 (2008).
- ⁸J. R. Maze, P. L. Stanwix, J. S. Hodges, S. Hong, J. M. Taylor, P. Cappellaro, L. Jiang, M. V. Gurudev Dutt, E. Togan, A. S. Zibrov, A. Yacoby, R. L. Walsworth, and M. D. Lukin, *Nature* **455**, 644 (2008).
- ⁹G. Balasubramanian, I. Y. Chan, R. Kolesov, M. Al-Hmoud, J. Tisler, C. Shin, C. Kim, A. Wojcik, P. R. Hemmer, A. Krueger, T. Hanke, A. Leitenstorfer, R. Bratschitsch, F. Jelezko, and J. Wrachtrup, *Nature* **455**, 648 (2008).
- ¹⁰P. Neumann, N. Mizuochi, F. Rempp, P. Hemmer, H. Watanabe, S. Yamasaki, V. Jacques, T. Gaebel, F. Jelezko, and J. Wrachtrup, *Science* **320**, 1326 (2008).
- ¹¹L. Childress, M. V. G. Dutt, J. M. Taylor, A. S. Zibrov, F. Jelezko, J. Wrachtrup, P. R. Hemmer, and M. D. Lukin, *Science* **314**, 281 (2006).
- ¹²Y. Kubo, F. R. Ong, P. Bertet, D. Vion, V. Jacques, D. Zheng, A. Dréau, J.-F. Roch, A. Auffeves, F. Jelezko, J. Wrachtrup, M. F. Barthe, P. Bergonzo, and D. Esteve, *Phys. Rev. Lett.* **105**, 140502 (2010).
- ¹³B. B. Buckley, G. D. Fuchs, L. C. Bassett, and D. D. Awschalom, *Science* **330**, 1212 (2010).
- ¹⁴N. Mohan, Y.-K. Tzeng, L. Yang, Y. Y. Chen, Y. Y. Hui, C. Y. Fang, and H. C. Chang, *Adv. Mater.* **22**, 843 (2010).
- ¹⁵E. Rittweger, K. Y. Han, S. E. Irvine, C. Eggeling, and S. W. Hell, *Nature Photonics* **3**, 144 (2009).
- ¹⁶H. Huang, E. Pierstoff, E. Osawa, and D. Ho, *Nano Lett.* **7**, 3305 (2007).
- ¹⁷T. Plakhotnik and D. Gruber, *PhysChemChemPhys* **12**, 9751 (2010).
- ¹⁸V. M. Acosta, E. Bauch, M. P. Ledbetter, A. Waxman, L.-S. Bouchard, and D. Budker, *Phys. Rev. Lett.* **104**, 070801 (2010).
- ¹⁹F. Dolde, H. Fedder, M. W. Doherty, T. Nöbauer, F. Rempp, G. Balasubramanian, T. Wolf, F. Reinhard, L. C. L. Hollenberg, F. Jelezko, and J. Wrachtrup, *Nature Physics* **7**, 459 (2011).
- ²⁰C. Bradac, T. Gaebel, N. Naidoo, M. J. Sellars, J. Twamley, L. J. Brown, A. S. Barnard, T. Plakhotnik, A. V. Zvyagin, and J. R. Rabeau, *Nature Nanotechnol.* **5**, 345 (2010).
- ²¹J. Botsoa, T. Sauvage, M. P. Adam, P. Desgardin, E. Leoni, B. Courtois, F. Treussart, and M. F. Barthe, *Phys. Rev. B* **84**, 125209 (2011).
- ²²F. C. Waldermann, P. Olivero, J. Nunn, K. Surmacz, Z. Y. Wang, D. Jaksch, R. A. Taylor, I. A. Walmsley, M. Draganski, P. Reichart, A. D. Greentree, D. N. Jamieson, and S. Praver, *Diamond Rel. Mater.* **16**, 1887 (2007).
- ²³Y.-R. Chang, H.-Y. Lee, K. Chen, C.-C. Chang, D.-S. Tsai, C.-C. Fu, T.-S. Lim, Y.-K. Tzeng, C.-Y. Fang, C.-C. Han, H.-C. Chang, and W. Fann, *Nature Nanotech.* **3**, 284 (2008).
- ²⁴V. M. Acosta, E. Bauch, M. P. Ledbetter, C. Santori, K.-M. C. Fu, P. E. Barclay, R. G. Beausoleil, H. Linget, J. F. Roch, F. Treussart, S. Chemerisov, W. Gawlik, and D. Budker, *Phys. Rev. B* **80**, 115202 (2009).
- ²⁵P. G. Baranov, A. A. Soltamova, D. O. Tolmachev, N. G. Romanov, R. A. Babunts, F. M. Shakhov, S. V. Kidalov, A. Y. Vul, G. V. Mamin, S. B. Orlinskii, and N. I. Silkin, *Small* **7**, 1533 (2011).
- ²⁶B. R. Smith, D. W. Inglis, B. Sandnes, J. R. Rabeau, A. V. Zvyagin, D. Gruber, C. J. Noble, R. Vogel, E. Ōsawa, and T. Plakhotnik, *Small* **5**, 1649 (2009).
- ²⁷B. R. Smith, D. Gruber, and T. Plakhotnik, *Diamond Rel. Mater.* **19**, 314 (2010).
- ²⁸T. Plakhotnik and R. Chapman, *New J. Phys.* **13**, 045001 (2011).
- ²⁹P. Neumann, R. Kolesov, V. Jacques, J. Beck, J. Tisler, A. Batalov, L. Rogers, N. B. Manson, G. Balasubramanian, F. Jelezko, and J. Wrachtrup, *New J. Phys.* **11**, 013017 (2009).
- ³⁰N. B. Manson, J. P. Harrison, and M. J. Sellars, *Phys. Rev. B* **74**, 104303 (2006).
- ³¹P. Delaney, J. C. Greer, and J. A. Larsson, *Nano Lett.* **10**, 610 (2010).
- ³²J. R. Maze, A. Gali, E. Togan, Y. Chu, A. Trifonov, E. Kaxiras, and M. D. Lukin, *New J. Phys.* **13**, 025025 (2011).
- ³³M. W. Doherty, N. B. Manson, P. Delaney, and L. C. L. Hollenberg, *New J. Phys.* **13**, 025019 (2011).
- ³⁴Y. Ma, M. Rohlfing, and A. Gali, *Phys. Rev. B* **81**, 041204(R) (2010).
- ³⁵A. Gali, M. Fyta, and E. Kaxiras, *Phys. Rev. B* **77**, 155206 (2008).
- ³⁶Kai-Mei C. Fu, C. Santori, P. E. Barclay, L. J. Rogers, N. B. Manson, and R. G. Beausoleil, *Phys. Rev. Lett.* **103**, 256404 (2009).
- ³⁷R. J. Epstein, F. M. Mendoza, Y. K. Kato, and D. D. Awschalom, *Nature Physics* **1**, 94 (2005).
- ³⁸L. J. Rogers, R. L. McMurtrie, M. J. Sellars, and N. B. Manson, *New J. Phys.* **11**, 063007 (2009).
- ³⁹N. D. Lai, D. Zheng, F. Jelezko, F. Treussart, and J.-F. Roch, *Appl. Phys. Lett.* **95**, 133101 (2009).
- ⁴⁰Y. Dumeige, F. Treussart, R. Alleaume, T. Gacoin, J.-F. Roch, and P. Grangier, *J. Lumin.* **109**, 61 (2004).
- ⁴¹N. B. Manson and J. P. Harrison, *Diamond Relat. Mater.* **14**, 1705 (2005).
- ⁴²T. Gaebel, M. Domhan, C. Wittmann, I. Popa, F. Jelezko, J. Rabeau, A. Greentree, S. Praver, E. Trajkov, P. R. Hemmer, and J. Wrachtrup, *Appl. Phys. B* **82**, 243 (2006).
- ⁴³D. A. Redman, S. Brown, R. H. Sands, and S. C. Rand, *Phys. Rev. Lett.* **67**, 3420 (1991).
- ⁴⁴P. Klan and J. Wirtz, *Photochemistry of Organic Compounds: From Concepts to Practice* (Wiley-Blackwell, Chichester, 2009).
- ⁴⁵D. M. Burland and G. W. Robinson, *Proc. Natl. Acad. Sci. USA* **66**, 257 (1970).
- ⁴⁶C. M. Marian, *WIREs Comput. Mol. Sci.* **2**, 187 (2012).
- ⁴⁷W. Lukosz and R. E. Kunz, *J. Opt. Soc. Am.* **67**, 1607 (1977).
- ⁴⁸P. Siyushev, H. Pinto, A. Gali, F. Jelezko, and J. Wrachtrup, *arXiv:1204.4898v1* (2012).
- ⁴⁹G. D. Fuchs, V. V. Dobrovitski, R. Hanson, A. Batra, C. D. Weis, T. Schenkel, and D. D. Awschalom, *Phys. Rev. Lett.* **101**, 117601 (2008).